Available online at www.sciencedirect.com
SCIENCE DIRECT®
Journal of Solid State Chemistry 178 (2005) 1712–1719
JOURNAL OF SOLID STATE CHEMISTRY
www.elsevier.com/locate/jssc

Effect of the synthesis conditions on the magnetic and electrical properties of the $BaFeO_{3-x}$ oxide: A metamagnetic behavior

Izaskun Gil de Muro, Maite Insausti, Luis Lezama, Teófilo Rojo*

Facultad de Ciencia y Tecnología, Departamento de Química Inorgánica, Universidad del País Vasco, UPV/EHU, Apdo, 644, Bilbao E-48080, Spain

Received 23 November 2004; received in revised form 11 March 2005; accepted 18 March 2005

Abstract

The $BaFeO_{2.95}$ oxide has been obtained from thermal decomposition of the $[BaFe(C_3H_2O_4)_2(H_2O)_4]$ metallo-organic precursor at 800 °C under atmospheric oxygen pressure as small and homogeneous particles. From electronic paramagnetic resonance data, a metallic behavior in the 230–130 K temperature range has been observed. Magnetic measurements confirm the existence of a ferro-antiferromagnetic transition at 178 K. The magnetic properties of the $BaFeO_{2.95}$ oxide are strongly dependent on both temperature and magnetic field with a metamagnetic behavior. The synthesis conditions play an important role on the morphology and the electrical and magnetic properties. The syntherization of the sample produces a dramatic change in the transport properties and the existence of conductivity disappears.

Keywords: Metallo-organic precursors; Mixed oxides; Antiferromagnet; Metamagnetism

1. Introduction

The study of perovskite-related mixed oxides has raised a high interest due to the variety of their magnetic and electrical properties. In the case of the $BaMO_{3-x}$ (M = Mn, Fe, Co) oxides, the high size of the Ba^{2+} cation and its basic nature allow the presence of transition metallic cations in high oxidation states (+III, +IV). These kinds of oxides usually exhibit hexagonal stacking of the perovskite structure, where chains of face-sharing octahedra running parallel to the c-axis with short $M-M$ distances. With increasing the size of the M metallic cation, cubic arrangement also appears, breaking the chains of face-sharing octahedra and showing a clear example of polytypism [1–3]. The oxygen-deficient phases tend to adapt the anionic vacancies through oxygen-deficient cubic layers. Face-sharing octahedra are not very usual in ionic solids and present the possibility of achieving magnetic arrangements at high temperatures and anomalous electrical properties [4], as it permits very strong M–O–M exchange interactions.

The iron perovskite-related oxides have been mainly investigated in relation to their electrical properties. The barium ferrates comprise a series of compositions exhibiting a wide range of oxygen deficiency. The more oxidized members in the $BaFeO_{3-x}$ system have been only obtained under high oxygen pressures and basically crystallize in the hexagonal system with presence of face-sharing and corner-sharing octahedra [5]. All of them show antiferromagnetic interactions together with a semiconductor behavior by hopping. In the case of the $BaFeO_{2.95}$ phase, a magnetic study carried out some years ago proposed a change in the electrical properties, simultaneous to a ferri-antiferromagnetic transition [6,7]. The phases with greater oxygen deficiency exhibit larger lattice parameters and smaller transition temperatures. It has been proposed that the magneto-electrical properties of these phases come determined by the indirect interaction between the iron cation and the oxygen anion in the lattice. If this interaction is weak the

*Corresponding author. Fax: +34 94 6013500.
E-mail address: qiproapt@lg.ehu.es (T. Rojo).

0022-4596/$ - see front matter © 2005 Elsevier Inc. All rights reserved.
doi:10.1016/j.jssc.2005.03.028

carriers will be move in the lattice by a hopping-like mechanism. Thus, the degree of the Fe–O–Fe interaction directly affects the carriers mobility and therefore the conductivity, which is directly influenced by the presence of oxygen vacancies and the Fe–O–Fe distances and angles in the chain [8].

The synthetic method used in the attainment of these phases plays an important role in the properties of these materials. The use of metallo-organic precursors has been shown to be an alternative method to the ceramic one in the preparation of mixed oxides [9,10]. Thermal treatments at controlled atmospheres of heteronuclear precursors yield the required oxide. Using this method, the reduction of the diffusion distances allows us to prepare highly homogeneous phases with small grain size, at shorter heating times and lower temperatures than those applied by other methods [11,12].

In this paper, we present the synthesis of the $BaFeO_{2.95}$ oxide, obtained from the $[BaFe(C_3H_2O_4)_2(H_2O)_4]$ metallo-organic precursor at 800 °C at atmospheric oxygen pressure. It is worth mentioning that the more oxidized oxides were only obtained under at high oxygen pressures and temperatures. We also describe the magnetic and electrical properties, and the influence of the soft synthesis conditions on these properties. In this sense, a sharp ferro-antiferromagnetic transition at 178 K together with a metallic behavior in the 230–130 K range have been observed. Furthermore, a strong field dependency of the magnetic properties with the existence of a metamagnetic behavior not reported until now, has been found.

2. Experimental section

2.1. Synthesis

The $[BaFe(C_3H_2O_4)_2(H_2O)_4]$ precursor was obtained as described in Ref. [13]. The analysis of the C, H and metals is consistent with the following stoichiometry: $BaFeC_6H_{12}O_{12}$ (Found: C, 15.56; H, 2.91; Fe, 12.06: Ba, 29.83 and calculated: C, 15.35; H, 2.58; Fe, 11.90: Ba, 29.26). Indexation of the powder diffraction pattern and refinement of the cell parameters confirm the presence of only one phase which is isostructural with the $[SrCu(C_3H_2O_4)_2(H_2O)_4]$ compound [14]. The $[BaFe(C_3H_2O_4)_2(H_2O)_4]$ precursor was initially fired in air at 400 °C, for 10 h, to remove the organic part. Then, thermal treatments at 800 °C in oxygen atmosphere gave rise to the formation of the $BaFeO_{2.95}$ oxide. The oxidation state of iron was determined by a titration method. The samples were dissolved under nitrogen in a solution of HCl, which reacts with metals in the formal +4 oxidation state to give Fe^{3+}. The evolving gas is collected in a solution of KI and after that, titrated with thiosulfate [15].

2.2. Physical measurements

Thermogravimetric measurements were performed in a Perkin Elmer System-7 DSC-TGA instrument. Crucibles containing 20 mg of sample were heated at 5° min^{-1} under dry nitrogen and air atmospheres. X-ray diffraction patterns were collected at room temperature on Philips X'Pert diffractometer equipped with graphite-monochromated using Cu$K\alpha_1$ radiation. Data were collected by scanning in the range $10° < 2\theta < 120°$ with increments of 0.02°(2θ). The structure was refined by the Rietveld method using the FULLPROF program. Scanning electron microscopic (SEM) and transmission electron microscopic (TEM) photographs using a JEOL JSM-6400 and a Philips CM200, respectively, were carried out. Magnetic and resistance measurements were performed in the temperature range 1.8–300 K using a QUANTUM DESIGN MPMS-7 SQUID magnetometer. The magnetic measurements were performed at magnetic fields between 0 and 7 T. Magnetic measurements at higher temperatures (300–900 K) were carried out in a Manics DSM-8 Faraday magnetometer. The resistance vs. temperature measurements were carried out by means of a *dc* four-probe system with the current parallel to the applied field. Electron paramagnetic resonance spectra were recorded on a Bruker ESP300 spectrometer, equipped with standard Oxford low-temperature devices operating at X band. The magnetic field was measured with a Bruker BNM 200 Gaussmeter, and the frequency was determined by using a Hewlett-Packard 5352B microwave frequency counter.

3. Results and discussion

3.1. Thermal analysis of the precursors

The thermal decomposition steps of the $[BaFe(C_3H_2O_4)_2(H_2O)_4]$ precursor were obtained from the TG curves shown in Fig. 1(a). It can be seen the occurrence of three consecutive processes: dehydration, ligand pyrolysis and inorganic residue formation. The first process takes place in the 75–175 °C range and corresponds to the loss of the four water molecules. After that, the decarboxylation of the ligand comes and a sharp mass loss in the temperature range 275–450 °C is observed. The measured weight losses agree with the formation of $BaCO_3$ and Fe_2O_3. Finally, a gradual mass loss is observed at temperatures above 600 °C, when carbonate decomposes and leads to the attainment of the mixed oxide. At this stage, the applied atmosphere plays an important role. In this way, the $BaFeO_{3-x}$ mixed oxide was obtained in the inorganic residue

in air atmosphere, whereas $Ba_2Fe_2O_5$ oxide together with some barium carbonate appears in the residue obtained in nitrogen atmosphere.

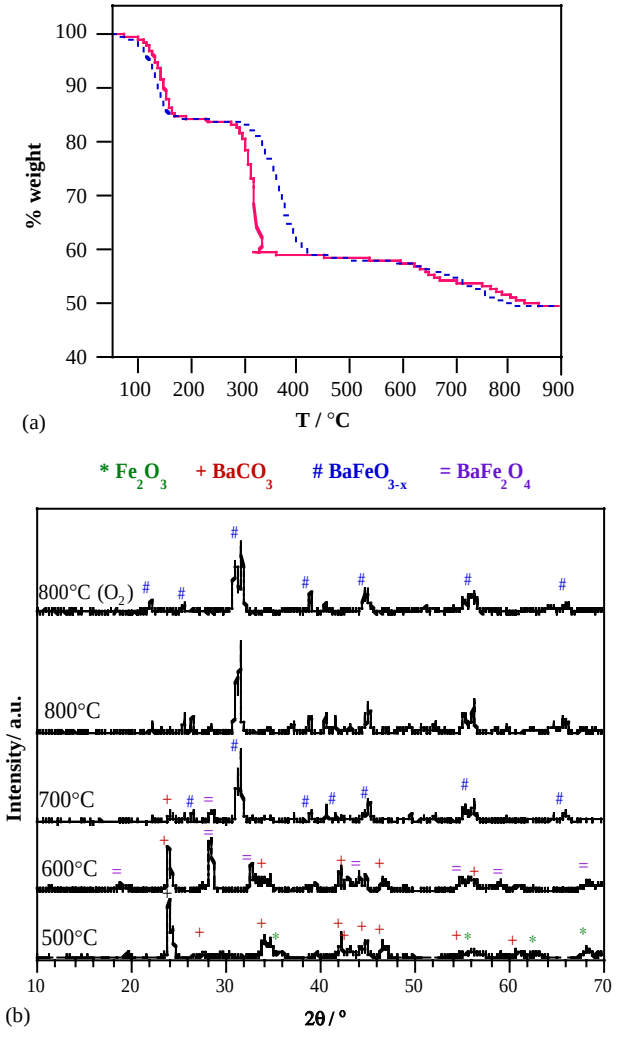

Fig. 1. (a) TG curves of BaFe precursor, under air (——) and nitrogen (·····) atmospheres. (b) XRD patterns of the phases obtained from the thermal treatment.

3.2. Formation of the mixed oxide

Following this study and in order to obtain a pure phase of the mixed oxide, thermal treatments under controlled atmosphere were carried out. After firing the BaFe malonate precursor at 400 °C, treatments at higher temperatures and different atmospheres were performed. The resulting products in each stage were characterized by X-ray powder diffraction (see Fig. 1b). The thermal decomposition of the $[BaFe(C_3H_2O_4)_2(H_2O)_4]$ precursor from 700 °C gave rise to the formation of the $BaFeO_{3-x}$ mixed oxide [16] together with some impurities. Finally, and in order to avoid the formation of the $BaFe_2O_4$ oxide [17], a thermal treatment at 800 °C in oxygen atmosphere was necessary. Taking into account these results, a pure phase of the $BaFeO_{3-x}$ oxide was obtained after firing the BaFe precursor in two steps, firstly at 400 °C for 12 h and secondly at 800 °C in oxygen atmosphere ($PO_2 = 1$ atm) for 15 h. The oxygen stoichiometry of the sample was measured by chemical titration. The results obtained indicate an approximately +3.90(8) oxidation state for the iron in the sample.

An SEM and TEM photographs were carried out to get some information about the morphology and the oxide compactness (Fig. 2). The photographs reveal uniform and fine grain growth, with very small, around 300 nm, and highly homogeneous particles. This morphology is a consequence of the soft synthesis route that favors the formation of small size particles, because the lower the temperature the smaller the size of the particles obtained. In addition, and considering that small grain sizes with higher surface areas are related to high degrees of reactivity, an easier oxygen absorption could explain the attainment of the oxide with a high oxygen content at oxygen pressures lower than those reported in the literature using the ceramic conditions [7,18].

The structure was refined by the Rietveld method using the FULLPROF program [19] (Fig. 3). Initially,

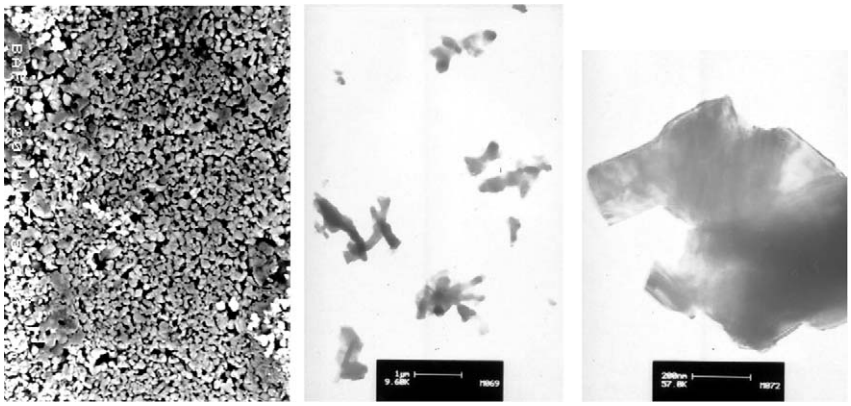

Fig. 2. SEM (× 5000) and TEM (× 10,000 and × 57,000) photographs of the $BaFeO_{2.95}$ oxide.

the X-ray powder diffraction pattern was indexed on the basis of the hexagonal group, $P6_3/mmc$, using the initial atomic positions proposed by Jacobson [20]. This is known as 6*H* phase, which may be described as face-shared pairs of FeO_6 octahedra corner linked to one FeO_6 octahedra. Nevertheless, some small peaks did not fit with this model and a second phase, known as 10*H* [21], was included in the refinement. The estimated percentage for the 10*H* phase being less than 6%. Considering the effect of this 10*H*-$BaFeO_{2.8}$ ($Fe^{+3.6}$) phase on the stoichiometry of our sample, the average iron oxidation state in the 6*H* main phase would be slightly higher, with the new stoichiometry 6*H*-$BaFeO_{2.97}$ ($Fe^{+3.94}$).

The refined parameters and selected bond lengths and angles corresponding to the 6*H* phase are summarized in Tables 1–3. Unfortunately, the accuracy of the data is not very good. The positions of the oxygen atoms have not been refined, so these results must be taken with caution. In the 6*H* majority phase, all iron atoms are octahedrally coordinated. Two $Fe(2)O_6$ face-sharing polyhedra are bounded through three O(1) atoms to form $Fe(2)_2O_9$ dimers, with Fe(2)–O(1)–Fe(2) angles between 87.3° and 87.4°. The $Fe(1)O_6$ octahedra share three O(2) atoms with other three $Fe(2)O_6$ polyhedra, the Fe(1)–O(2)–Fe(2) angle being of 175.6°. The average Fe(1)–O distances are 2.01 Å, and the average values for Fe(2)–O(1) and Fe(2)–O(2) in the face-sharing polyhedra are 1.95 and 1.89 Å, respectively.

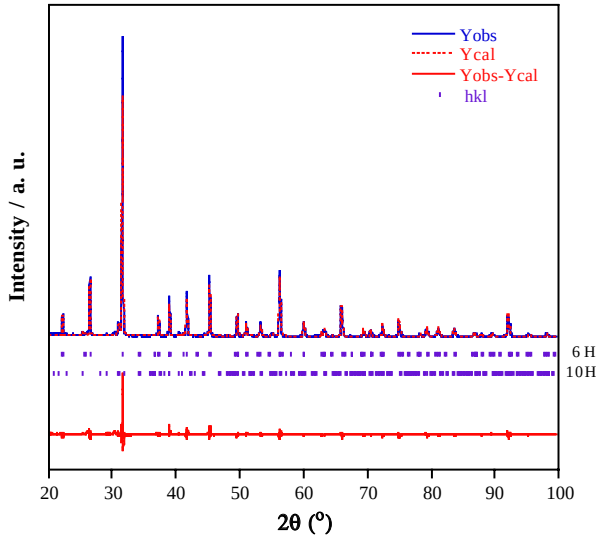

Fig. 3. X-ray powder diffraction data and Rietveld refinement profile for $BaFeO_{2.95}$.

3.3. Spectroscopic, magnetic and electrical properties

The powdered X band EPR spectra measured at different temperatures are represented in Fig. 4. An isotropic broad signal centered at $g \approx 2$ with a linewidth $\Delta Hpp = 850$ G appears at room temperature. The linewidth diminishes with decreasing temperature until

Table 2
Refined atomic positional parameters

Phase 6H	*x*	*y*	*z*	Biso	occ.
Ba(1)	0	0	1/4	1.06(5)	0.083
Ba(2)	1/3	2/3	0.5902(1)	1.43(4)	0.167
Fe(1)	0	0	0	0.8(1)	0.083
Fe(2)	1/3	2/3	0.1531(3)	1.6(1)	0.167
O(1)	0.47717	0.95408	1/4	1	0.224
O(2)	0.16800	0.33600	0.41660	1	0.499
Phase 10H	*x*	*y*	*z*	$B_{overall}$	occ.
Ba(1)	0	0	1/4		0.083
Ba(2)	1/3	2/3	0.3685(8)		0.167
Ba(3)	1/3	2/3	0.9635(7)		0.167
Fe(1)	0	0	0.611(1)		0.167
Fe(2)	1/3	2/3	0.818(2)	0.7(2)	0.167
Fe(3)	0	0	0		0.083
O(1)	0.3298	0.1649	0.35075		0.224
O(2)	0.7051	0.8225	0.45441		0.500
O(3)	1/3	2/3	3/4		0.500
O(4)	1/3	2/3	1/4		0.083

*O positions are not refined.

Table 3
Selected Fe–O (Å) distances and Fe–O–Fe angles (deg) in the 6*H* majority phase

$Fe(1)O_6$	Fe(1)–O(2)	2.016 (x2) 2.014 (x4)	O(2)–Fe(1)–O(2)	89.7–90.3
$Fe(2)O_6$	Fe(2)–O(1)	1.951 (x2) 1.950	O(1)–Fe(2)–O(1)	77.5–77.6
	Fe(2)–O(2)	1.890 1.887 (x2)	O(2)–Fe(2)–O(2)	96.2–96.3
			O(1)–Fe(2)–O(2)	92.3–92.4 167.1
	Fe(1)–O(2)–Fe(2)	175.6	Fe(2)–O(1)–Fe(2)	87.3–87.4
	Fe(2)…Fe(2)	2.695		

Table 1
Refined cell parameters and reliability factors

	Space group	*a* (Å)	*c* (Å)	*V* (Å^3)	χ^2	R_{wp} (%)	R_p (%)
Phase 6*H*	$P6_3/mmc$	5.671 (1)	13.873(2)	386.1 (2)	3.93	21.2	12.7
Phase 10*H*	$P6_3/mmc$	5.784 (7)	24.63 (3)	719 (1)			

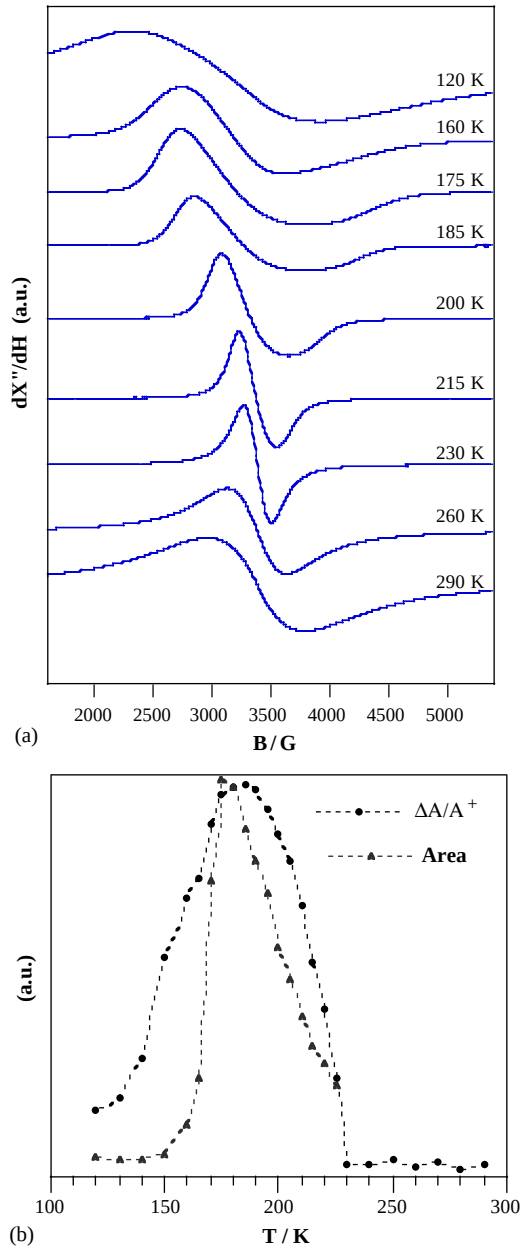

Fig. 4. (a) Powder X-band EPR spectra at different temperatures for the $BaFeO_{2.95}$ oxide. (b) Thermal evolution of the anisotropy ($\Delta A/A^{+}$) and of the area for EPR signals.

230 K, as the spin-lattice relaxation time increases. In the 200–160 K temperature range, an anomalous line shape is observed. The symmetric Lorentzian profile changes to an asymmetric Dysonian line which is characteristic of conductive materials [22]. The anisotropy of the signals has been studied by representing $\Delta A/A^{+}$ vs. T, where ΔA is the difference between the amplitude of the positive (A^{+}) and negative (A^{-}) lobule (see Fig. 4b). As can be seen, the anisotropy drastically changes in the 230–130 K temperature range, and the spectra show the characteristics of a metallic state. Below this temperature, the linewidth increases becoming electronic paramagnetic resonance (EPR) silent at 120 K. This fact can be attributed to the presence of long-range antiferromagnetic interactions in this system.

Taking into account that the area is related to the magnetic susceptibility and therefore to the magnetic moment, we have also represented the thermal variation of the area. The curve shows the presence of a maximum at 175 K, which corresponds to that observed in the magnetic moment, indicating that the T_N value is close to 175 K.

The magnetic susceptibility measurements performed in the temperature range 4.2–800 K are represented in Fig. 5. A sharp peak appears at 178 K, indicating the presence of a ferro-antiferromagnetic transition at this temperature.

As can be seen, the magnetic moment at 300 K has not reached a constant value. This value decreases with temperature until 600 K, indicating the existence of some small ferromagnetic interactions at room temperature. The values obtained at high temperatures, 4.17 μB at 500 K, are slightly small for a system with majority of high spin Fe^{4+} ions. This fact can be attributed to the small contribution of the 10H-$BaFeO_{3-x}$ antiferromagnetic impurity (with a $T_{Néel} > 300$ K) that would induce a lower value for the magnetic moment than that expected [23]. In any case, as the sample is reduced with heating in a no-oxidant atmosphere, the data from the magnetic measurements at high temperatures must be taken with caution.

Magnetization loops vs. magnetic field measurements were also performed at different temperatures and the results are shown in Fig. 6. The linear dependence of the magnetization observed between 300 and 200 K confirms its nearly paramagnetic nature. Below 200 K, a sigmoidal curve characteristic of ferromagnetic systems appears. The coercive field is practically negligible and the magnetization (0.6–0.7 in $N\beta$ units) is smaller than that corresponding to an Fe^{4+}/Fe^{3+} system. This

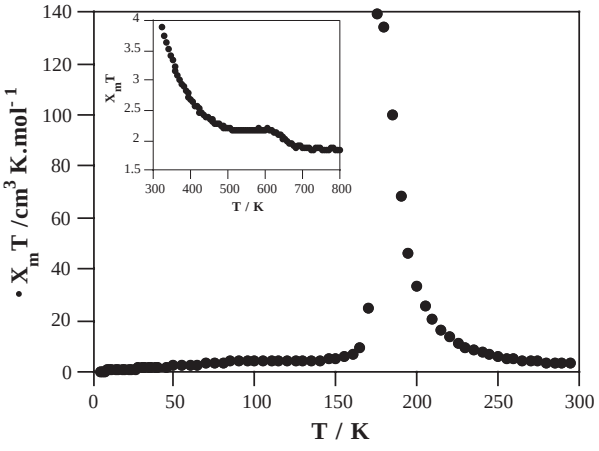

Fig. 5. $\chi_m T$ vs. T curves for the $BaFeO_{2.95}$ oxide.

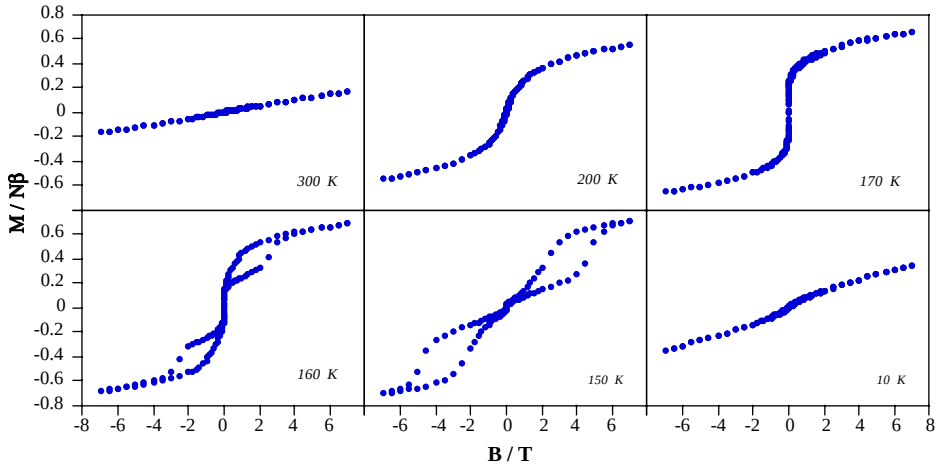

Fig. 6. M vs. B loops at different temperatures for the $BaFeO_{2.95}$ oxide.

sigmoidal curve shape observed between 200 and 170 K is consistent with the ferromagnetic component observed in the $\chi_m T$ curve. In the 170–140 K temperature range, the magnetization shows an unusual behavior, and a *quasi*-spontaneous spin alignment is observed. This effect is more pronounced at low temperatures, but a more intense applied field is needed to order the spins. In all cases, hysteresis loops with maxima magnetization values of 0.7 (in $N\beta$ units) are observed. That is, once the alignment is reached, it remains at lower fields than those needed to induce it. At temperatures below 140 K, this effect is not observed because higher magnetic fields should be necessary to be detected. The isothermal magnetization curves represented in Fig. 7 exhibit a sigmoidal shape between 170 and 140 K, indicating a discontinuous rise of the magnetization with the applied magnetic field. The transition takes place at higher fields with decreasing temperature but it is not observed below 140 K at high magnetic fields (7 T).

These curves are characteristic of a metamagnetic behavior. This can be observed in antiferromagnetic materials with a large magnetic anisotropy in the presence of competing ferromagnetic interactions. They can undergo a first-order transition to a phase in which a net magnetic moment exists [24]. In this sense, the structure and the Fe…Fe interactions are important factors to be considered in order to understand the magnetic properties of this oxide. As can be seen in Fig. 8, along the c-axis the two Fe(2) atoms from the face-sharing octahedra can interact via three O(1) oxygen atoms with angles around 87°. At the same time, each Fe(2) atom is connected with three Fe(1) through O(2) atoms with angles of 175.7°, along the c axis and the ab plane, extending the interactions in the three dimensions.

The ferromagnetic coupling is not very usual in this kind of oxides, but in our case, the presence of face-sharing octahedra with exchange angles less than 90°

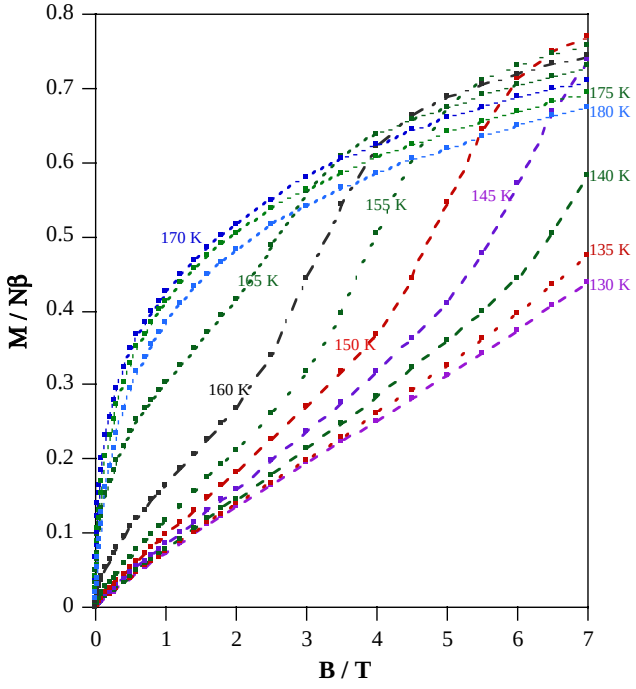

Fig. 7. Isothermal magnetization curves from 130 to 180 K for the $BaFeO_{2.95}$ oxide.

might induce a parallel alignment of the spins. At lower temperatures, the overall of the spin moments of the iron ions will be antiferromagnetically coupled but slightly canted as a consequence of the competition between different Fe–O–Fe interactions, producing a weak spontaneous magnetization. However, below 170 K, only a portion of the spins changes their orientation with the same magnetic field and the system lead to a metastable phase. This is characterized by the coexistence of two homogeneous paramagnetic and antiferromagnetic phases, in which the transition takes place gradually with increasing the magnetic field.

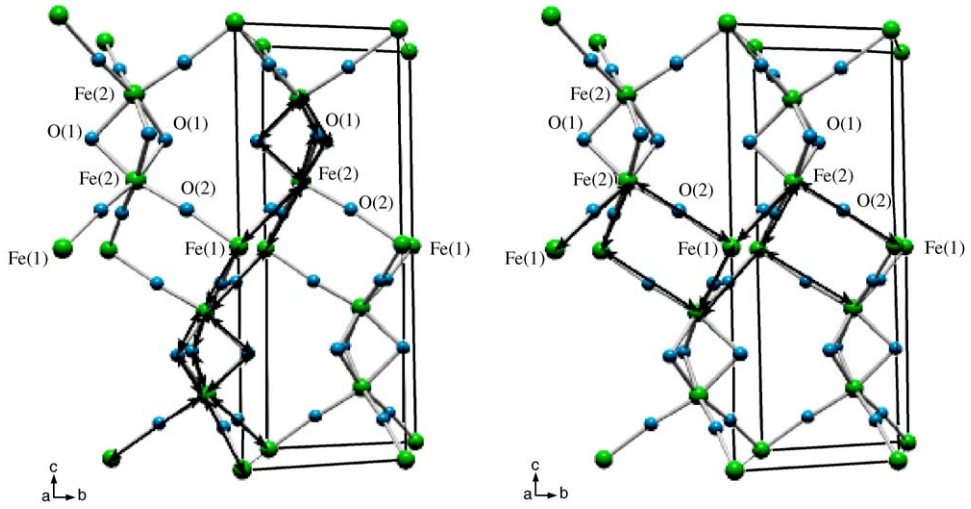

Fig. 8. Fe–O–Fe possible interactions in the 6*H* $BaFeO_{3-x}$ structure.

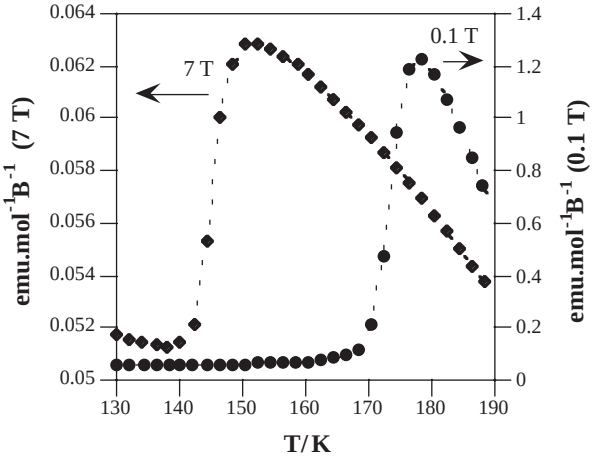

Fig. 9. M/B vs. *T* curves at 7 and 0.1 T for the $BaFeO_{2.95}$ oxide.

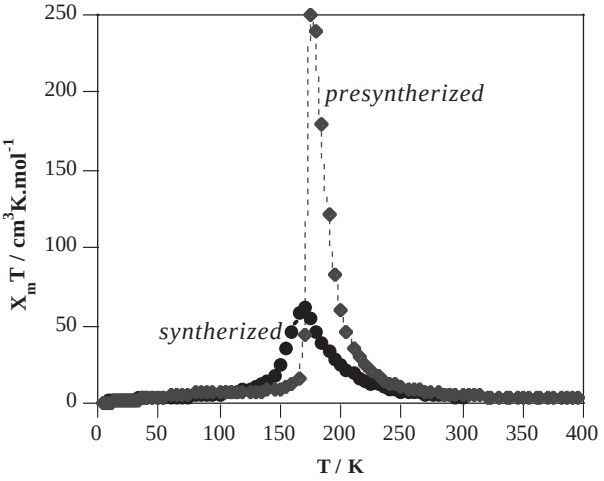

Fig. 10. $\chi_m T$ vs. *T* curves for the $BaFeO_{2.95}$ oxide, presyntherized and syntherized.

To study the effect of the applied magnetic field on the usual $\chi_m T$ vs. *T* curves, magnetization vs. *T* measurements at 0.1 and 7 T were also performed. The results are shown in Fig. 9. At low fields, the magnetic transition takes place at 178 K in good agreement with the $\chi_m T$ curve, but it is shifted up to 150 K at 7 T. The maximum value of the magnetic susceptibility drastically decreases from 1.2 emu mol^{-1} at 0.1 T down to 0.063 emu mol^{-1} at 7 T, indicating that strong magnetic fields difficult the establishment of the antiferromagnetic ordering and consequently, the ferro-antiferromagnetic transition.

This behavior is quite similar to that found by MacChesney et al. some years ago [7]. They observed (using a pendulum magnetometer and under a magnetic field of 15.3 kOe) that the $BaFeO_{2.95}$ phase, synthesized under high pressure of oxygen, was paramagnetic above 180 K, ferrimagnetic between 180 and 164 K and antiferromagnetic below 164 K. However, we have not observed any decrease in the $\chi_m T$ data previous to the ferromagnetic component and measurements at lower fields allowed us to observe the described metamagnetic behavior.

In order to study the thermal evolution of the resistivity, a pellet of the $BaFeO_{2.95}$ oxide was synthetized at 800 °C in oxygen atmosphere for 12 h to be measured in a *dc* four-probe system. Surprisingly, no changes in the resistivity values were detected with decreasing temperature, in disagreement with the EPR data. In this way, new EPR and magnetic measurements were carried out for the syntherized sample. The EPR spectra did not exhibit the previous anisotropic signals, showing the typical behavior of an antiferromagnet with a T_N near 160 K. The new magnetic measurements were also different and remarkable differences between the presyntherized and the syntherized samples appear (see Fig. 10). As can be seen, the transition temperature was

slightly lower and the maximum value of the $\chi_m T$ curve decreases significantly for the syntherized sample.

MacChesney et al. [7] had also observed a discontinuity in the resistivity data, simultaneous to the magnetic transition. This discontinuity disappears in our syntherized sample and a change in the magnetic properties is observed. This effect is probably related to the decrease in the oxygen content in the oxide, since the existence of oxygen vacancies difficult the Fe–O–Fe interaction along the sample, and consequently, lower values of the T_N temperature and weaker transition peaks are expected.

In order to see the effect of the synthetic conditions on the properties of this phase, several syntheses at different conditions were performed. It can be seen that the best conditions are in the 750–800 °C temperature range. Both the reaction times and the amount of product show a great influence on the stoichiometry of the obtained oxide. In this way, small amounts of product and reaction times of 10–15 h were needed. Longer reaction times give rise to small reductions and changes on the magnetoelectrical properties of the oxide.

4. Conclusions

The non-stoichiometric oxide, $BaFeO_{2.95}$, was obtained from thermal decomposition of the $[BaFe(C_3H_2O_4)_2(H_2O)_4]$ precursor in oxygen atmosphere at 800 °C. This is the first phase with a high degree of oxidation obtained at low oxygen pressures and temperatures. The use of the soft synthetic conditions gives rise to the attainment of a phase with homogeneous morphology and small grain size.

The compound presents a ferro-antiferromagnetic transition at 178 K. These competing interactions in an anisotropic magnetic structure lead to the occurrence of a metamagnetic behavior. In addition, differences in the shape and the transition temperature were observed when changing the applied magnetic field. Thus, it can be concluded that the magnetic properties are strongly dependent on both temperature and applied magnetic field.

The change of the EPR linewidth, from a symmetric Lorentzian profile to an asymmetric Dysonian line, indicates a conducting behavior in the 230–130 K temperature range. Nevertheless, longer reaction times lead to the disappearance of the conducting behavior and a change on the magnetic properties.

Finally, we can conclude that the synthetic method directly affects not only the morphology, but also the stoichiometry and the magneto-electrical properties of the $BaFeO_{3-x}$ oxide.

Acknowledgments

This work has been carried out with the financial support of the Ministerio de Ciencia y Tecnología MCyT (MAT2001-0064 and MAT2004-02425) and the Universidad del País Vasco/Euskal Herriko Unibertsitatea (9/UPV00169.310-14199/2001). The authors would also like to thank Prof. M.L. Nó for providing user time of the electronic microscopes.

References

[1] T. Negas, R.S. Roth, J. Solid State Chem. 3 (1971) 323;
J.M. González-Calbet, M. Parras, J.M. Alonso, M. Vallet-Regí, J. Solid State Chem. 99 (1993) 106;
J.M. González-Calbet, M. Parras, J.M. Alonso, M. Vallet-Regí, J. Solid State Chem. 111 (1994) 202.
[2] J.M. González-Calbet, M. Parras, J.M. Alonso, M. Vallet-Regí, J. Solid State Chem. 99 (1993) 106.
[3] J.M. González-Calbet, M. Parras, J.M. Alonso, M. Vallet-Regí, J. Solid State Chem. 111 (1994) 202.
[4] A.F. Wells, Structural Inorganic Chemistry, fifth ed, Clarendon Press, Oxford, 1984.
[5] J.C. Grenier, A. Wattiaux, M. Pouchard, P. Hagenmuller, M. Parras, M. Vallet, J. Calbet, M.A. Alario-Franco, J. Solid State Chem. 80 (1989) 6.
[6] P.K. Gallagher, J.B. MacChesney, D.N.E. Buchanan, J. Chem. Phys. 43 (2) (1965) 516.
[7] J.B. MacChesney, J.F. Potter, R.C. Sherwood, H.J. Williams, J. Chem. Phys. 43 (9) (1965) 3317.
[8] J. Hombo, Y. Matsumoto, T. Kawano, J. Solid State Chem. 84 (1990) 138.
[9] C.N.R. Rao, Chemical Approaches to the Synthesis of Inorganic Materials, Wiley, New York, 1994.
[10] K. Vidyasagar, J. Gopalakrishnan, C.N.R. Rao, Inorg. Chem. 23 (1984) 1206.
[11] F.F. Lange, in: L.L. Hench, J.K. West (Eds.), Chemical Processing of Advanced Materials, Wiley, New York, 1992.
[12] I. Gil de Muro, M. Insausti, L. Lezama, J.L. Pizarro, M.I. Arriortua, T. Rojo, Eur. J. Inorg. Chem. (1999) 935.
[13] I. Gil de Muro, L. Lezama, M. Insausti, T. Rojo, Eur. J. Inorg. Chem. (2003) 2948.
[14] I. Gil de Muro, F.A. Mautner, M. Insausti, L. Lezama, M.I. Arriortua, T. Rojo, Inorg. Chem. 37 (1998) 3243.
[15] B.E. Gushee, L. Katz, R. Ward, J. Am. Chem. Soc. 79 (1957) 5601.
[16] Powder Diffraction File, Card No. 23-1024. Joint Committee on Powder Diffraction Standars, Swarthmore, PA, 1995.
[17] Powder Diffraction File, Card No. 25-1191. Joint Committee on Powder Diffraction Standars, Swarthmore, PA, 1995.
[18] Y. Takeda, M. Shimada, F. Kanamaru, M. Koizumi, Mater. Res. Bull. 9 (1974) 537;
Y. Takeda, M. Shimada, F. Kanamaru, M. Koizumi, J. Solid State Chem. 7 (1973) 229.
[19] J. Rodríguez-Carvajal, Physica B 192 (1992) 55.
[20] A.J. Jacobson, Acta Crystallogr. B 32 (1976) 1087.
[21] M.I. Gomez, G. Lucotti, J.A. de Morán, P.J. Aymonino, S. Pagola, P. Stephens, R.E. Carbonio, J. Solid State Chem. 160 (2001) 17.
[22] F. Dyson, Phys. Rev. 98 (1955) 349.
[23] J.L. Delattre, A.M. Stacy, T. Siegrist, J. Solid State Chem. 177 (2004) 928.
[24] R.M. Carling, Magnetochemistry, Springer, Berlin, 1986.